ACS APPLIED NANO MATERIALS

www.acsanm.org Article

MoX_2 (X = O, S) Hierarchical Nanosheets Confined in Carbon Frameworks for Enhanced Lithium-Ion Storage

Xiue Zhang, Huajuan Ren, Bin Xie, Yatao Yan, Guowang Diao, Ming Chen,* and Shaowei Chen*

Cite This: *ACS Appl. Nano Mater.* 2021, 4, 4615−4622 Read Online

ACCESS | Metrics & More | Article Recommendations | Supporting Information

ABSTRACT: MoX_2 (X = O, S) layered structures are promising anode materials for lithium-ion batteries because of their intrinsically high theoretical capacity. Yet, the poor electrical conductivity and substantial volume change during reaction with Li^+ ions greatly limit their practical application. This can be mitigated by developing a proper carbon framework for effective confinement of the growth of active materials. Herein, a universal carbon framework template has been exploited for the synthesis of thin MoX_2 nanosheets encapsulated in mesoporous hollow carbon frameworks (MHCFs) by the confinement approach, forming a MoX_2/C interconnected network. The porous hierarchical architectures offer sufficient void space for MoX_2 nanosheets during the expansion process. Meanwhile, the confining effect of hollow carbon spheres can prevent aggregation and spreading out from the carbon of MoX_2 nanosheets to guarantee high structural integrity upon cycling (638 mA h g^{-1} for MoO_2/C at 1 A g^{-1} after the 1000th cycle and 525 mA h g^{-1} for MoS_2/C after 200 at 1 A g^{-1}).

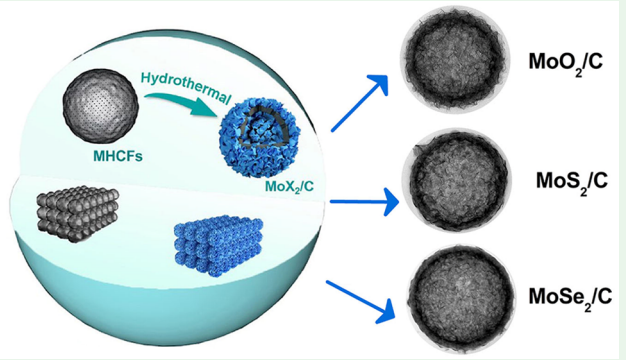

KEYWORDS: *MoX_2 layered structure, universal hollow mesoporous carbon framework, encapsulated hierarchical structure, confining effect, lithium-ion battery*

INTRODUCTION

Two-dimensional (2D) nanomaterials, such as graphene,[1,2] transition-metal dichalcogenides (e.g., MoS_2 and VS_2),[3−7] transition-metal oxides (e.g., MoO_2 and MnO_2),[8−13] transition-metal selenides (e.g., $MoSe_2$ and WSe_2),[14−16] and phosphides,[17] have attracted broad interest because of their unique crystal structures and material properties.[18−21] Among them, MoX_2 (X = O, S) layered nanostructures, with their high theoretical specific capacity, are the most promising compounds as efficient anode materials for LIBs.[22−26] Nonetheless, the large volume variations and poor conductivity of MoX_2 have been identified as critical roadblocks to the further development of lithium-ion batteries (LIBs).

These issues can be mitigated by incorporating the active materials into porous carbon frameworks,[27−31] and a range of molybdenum-based materials combined with carbon nanomaterials with different morphologies and nanostructures have been examined.[32−36] Generally, carbon components in the nanocomposite electrode are anticipated to effectively improve the electrical conductivity and alleviate volume changes upon cycling.[37−40] For example, see hierarchical hollow MoO_2/nitrogen-doped carbon,[41] MoO_2@C core−shell nanofibers,[42] MoS_2/Ti_3C_2-MXene,[43] hierarchical porous MoS_2/C nanospheres,[44] and V_4C_3-MXene/MoS_2/C.[45] Unfortunately, in these studies pulverization and aggregation tend to occur in the carbon-supported molybdenum-based materials upon cycling, which lead to the poor life and sluggish dynamics of lithium-ion storage. Hence, the development of a universal hollow carbon framework is of great importance for the growth of active materials.

Herein, we employ a universal carbon framework template to synthesize MoX_2/C (X = O, S) hierarchical nanospheres, which are composed of thin MoX_2 nanosheets encapsulated in mesoporous hollow carbon frameworks (MHCFs) with a simple hydrothermal method. The rationally designed hierarchically porous architecture contains abundant empty space and compliant backbones to mitigate the volume change effects upon cycling, facilitates rapid ion diffusion and transport throughout the entire structure, and provides interpenetrating conductive networks for electron transfer. Meanwhile, the confining effect of hollow carbon spheres can prevent aggregation and exfoliation. Electrochemical measurements show that the obtained MoX_2/C hierarchical nanospheres exhibit excellent energy storage performances of LIBs. Such a strategy can be extended to $MoSe_2$/C materials, which are

Received: January 23, 2021
Accepted: April 26, 2021
Published: May 6, 2021

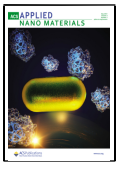

similar to the $MoSe_2$/C composite synthesized using hard-template methods.[46,47]

RESULTS AND DISCUSSION

The formation process of MoX_2/C hierarchical nanospheres is schematically illustrated in Figure 1a (details in the Supporting Information). MHCFs were first synthesized by adopting a surfactant-free procedure based on the self-assembly of tetraethyl orthosilicate and resorcinol–formaldehyde, followed by thermal annealing and chemical etching of SiO_2 (Figure S1).[32] Scanning electron microscopy (SEM) measurements show that MHCFs exhibit a smooth spherical shape of around 400 nm diameter (Figure 1b). Consistent results were obtained with transmission electron microscopy (TEM) measurements, where MHCFs can be seen to exhibit a hollow structure with a porous carbon shell of about 20 nm thickness (Figure 1c,d). After hydrothermal treatment, thin MoO_2 nanosheets were then encapsulated in the prepared MHCFs through a simple hydrothermal method, producing MoO_2/C hierarchical nanocomposites. The smooth surface of the carbon spheres became rough because of the MoO_2 nanosheets anchored on the carbon sphere surface, as evidenced in SEM (Figure S2a,b) and TEM (Figures 1e and S2c,d) measurements. Correspondingly, the diameter of the MoO_2/C hierarchical composite increases to ca. 420 nm. Excitingly, the prepared hollow carbon framework template is universal and can also be used for the synthesis of MoS_2/C and $MoSe_2$/C hierarchical nanospheres (Figures 1f,g and S3 and S4).

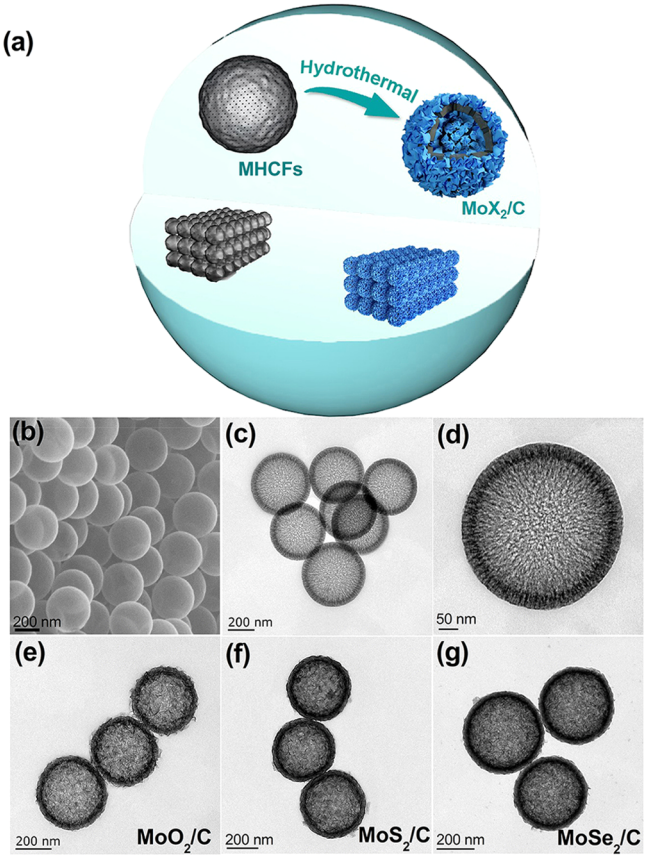

Figure 1. (a) Schematic illustration of the preparation of MoX_2/C composites. (b) SEM and (c and d) TEM images of MHCFs. TEM images of (e) MoO_2/C, (f) MoS_2/C, and (g) $MoSe_2$/C.

Additionally, it is worth noting that hollow carbon frameworks act as templates in the confined growth of active components.

To reveal the distribution of MoO_2 nanosheets in the internal cavity of MHCFs, TEM images were acquired with the top and bottom parts of the hierarchical MoO_2/C composites microtomed off. As shown in Figure 2a, the MoO_2 nanosheets were mainly encapsulated in the hollow cores, and a small amount of them was found within the carbon shells and exterior surfaces. A comparison between the hollow (highlighted by the yellow circles) and filled structures after the cutting treatment further proved the filling with the MoO_2 nanosheets. The formation of a MoX_2/C structure is further confirmed by elemental mapping analysis based on energy-dispersive X-ray (EDX) spectroscopy. The MoO_2/C and MoS_2/C composites can be seen to entail C, Mo, and O (Figure 2b–e) and C, Mo, and S (Figure S5a–d), and the above elements are enriched at the edge of the nanospheres. In addition, the line scan further confirms the spatial distributions of C, Mo, O, or S along the lengthwise direction of the hollow carbon sphere (Figures 2f and S5e). High-resolution TEM (HRTEM) measurements indeed indicate that the carbon shells are decorated with ultrathin nanosheets (Figures 2g,g1 and Figure S5f1,f2). Figures 2g2 and S5f2 reveal the formation of a large number of exposed MoO_2 and MoS_2 nanosheets with thicknesses of 2–5 layers. Meanwhile, the porous structure was confirmed by Brunauer–Emmett–Teller (BET) measurements of MoO_2/C and MoS_2/C, with specific surface areas of 100.6 and 138.4 $m^2\ g^{-1}$, respectively (pore size ranges from 1.8 nm to 4 and 2.2 nm, respectively; Figure S6), which was conducive to electrolyte ion transport and reaction kinetics.[48−50] For comparison, unsupported pure MoO_2 and MoS_2 nanosheets exhibit an irregular morphology and were made up of micron-sized sheets, with markedly lower BET surface areas of 38.2 and 54.2 $m^2\ g^{-1}$ for pure MoO_2 and pure MoS_2 (Figure S9). The contents of carbon in MoO_2/C and MoS_2/C calculated from the thermogravimetric analysis (TGA) curves (Figure S10) were about 14.0 and 14.6 wt %, respectively.

Figure 3a shows the crystallinity and composition of pure MoO_2 and hierarchical MoO_2/C nanospheres by X-ray diffraction (XRD). Both samples exhibit a series of well-defined diffraction peaks at 2θ = 26.1°, 36.8°, 41.3°, 53.4°, 60.3°, and 66.4°, which can be assigned to the (−111), (111), (210), (−312), (031), and (202) planes of a monoclinic MoO_2 crystal (JCPDS 32-0671).[41,50] Note that the carbon patterns in hierarchical MoO_2/C are likely overshadowed by the strong signals of MoO_2. In Raman spectroscopic measurements (Figure 3b), both samples displayed two major vibrational peaks centered at 818 and 992 cm^{-1} that can be indexed to ν(Mo–O–Mo stretch) and ν(Mo=O stretch) of MoO_2.[51,52] In addition, MoO_2/C also exhibits two vibrational bands at 1392 and 1602 cm^{-1} due to the D and G bands of graphitic carbon (MHCFs), respectively.[53]

The elemental composition and valence state of the MoO_2/C composite are then analyzed by XPS measurements. In the XPS spectrum (Figure 3c), five distinct peaks can be identified at 231.9 eV (Mo 3d), 284.0 eV (C 1s), 397.2 eV (Mo $3p_{3/2}$), 414.2 eV (Mo $3p_{1/2}$), and 529.9 eV (O 1s), consistent with the elemental composition of MoO_2/C.[52] From the high-resolution scan of the Mo 3d electrons (Figure 3d), deconvolution yields two doublets at 228.4/231.7 and 230.0/234.6 eV, due to the $3d_{5/2}$ and $3d_{3/2}$ electrons of Mo^{IV} and Mo^{VI}, respectively. The former is consistent with the formation

https://doi.org/10.1021/acsanm.1c00218
ACS Appl. Nano Mater. 2021, 4, 4615–4622

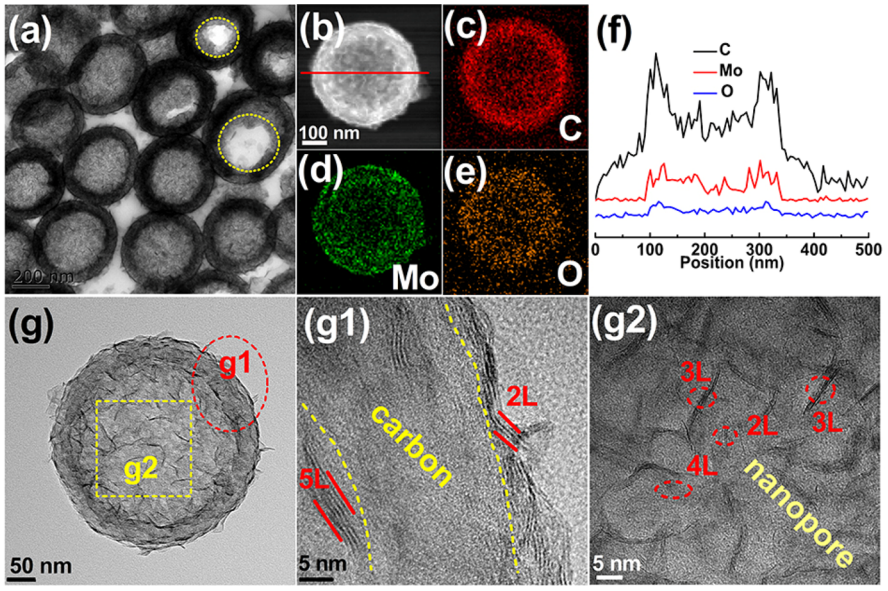

Figure 2. (a) TEM image of a MoO_2/C cross section after microtoming. (b–e) Annular dark-field scanning TEM images and the corresponding EDX elemental maps of C, Mo, and O. (f) EDX line-scan profiles and (g, g1, and g2) HRTEM images of MoO_2/C.

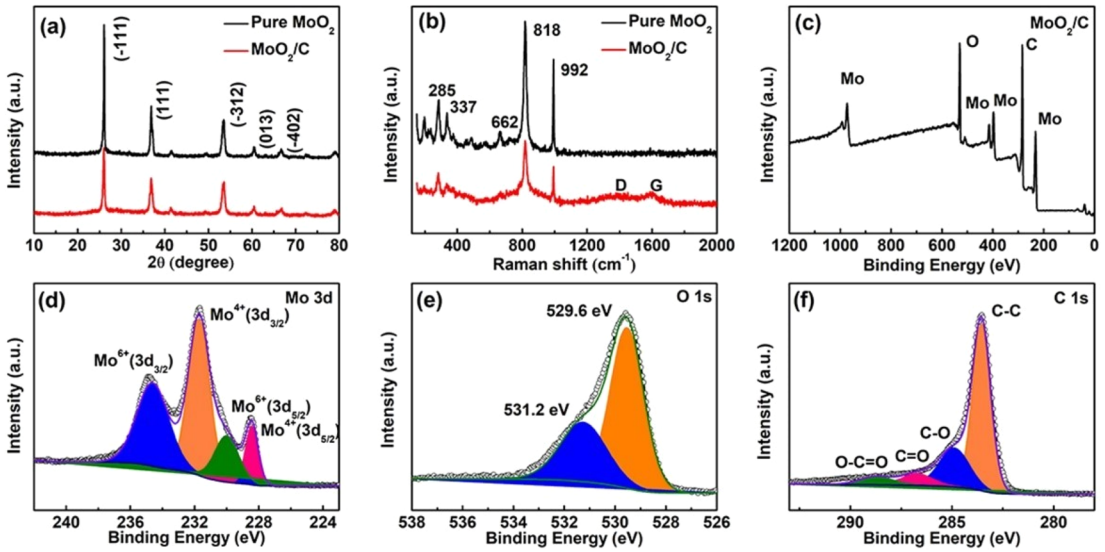

Figure 3. (a) XRD patterns and (b) Raman spectra of MoO_2/C composites and pure MoO_2. (c) XPS survey spectrum and (d–f) high-resolution scans of the (d) Mo 3d, (e) O 1s, and (f) C 1s electrons of the MoO_2/C composites.

of MoO_2, whereas the latter likely arises from the surface oxidation of metastable MoO_2 into MoO_3.[54,55] In the O 1s spectrum (Figure 3e), two peaks can be resolved, where the main peak at 529.6 eV corresponds to oxygen in Mo–O, whereas the minor one at 531.2 eV is due to residual oxygen-containing groups bonded with carbon in the hollow carbon spheres. In the C 1s spectrum (Figure 3f), four components can be resolved, pointing to C–C (283.5 eV), C–O (285.0 eV), C═O (286.7 eV), and O–C═O (288.5 eV).[56,57]

The electrochemical performance for Li^+ storage by the obtained nanocomposites was assessed with a CR2032 coin cell. Parts a and b of Figure 4 show the four initial cyclic voltammetry (CV) measurements of the MoO_2/C and pure MoO_2 electrodes under a potential scan rate of 0.1 mV s^{-1}. At the positions of 0.68, 1.25, and 1.51 V, three reduction peaks appeared in the first cycle, respectively. The two peaks that appeared at 1.51 and 1.25 V suggest that the Li^+ inserts into MoO_2 to form $Li_{x_1}MoO_2$ and $Li_{x_2}MoO_2$ ($x_2 > x_1$). This process was accompanied by phase transformation. It is worth noting that a broad irreversible peak that appeared at 0.68 V is associated with irreversible side reactions and the formation of a solid electrolyte interphase,[58] which disappeared during subsequent cycles. Two oxidation peaks appeared at 1.4–1.7 V, indicating the oxidation of Mo^0 to Mo^{4+} and the decomposition of Li_2O.[59] Two redox couples (1.51/1.71 and 1.25/1.42 V) were observed during subsequent cycles, which are attributed to the transformation of molybdenum oxides between the monoclinic and orthorhombic phases caused by the insertion/extraction of lithium ions.[60] The lithium insertion mechanism is based on the following conversion:

$$MoO_2\ (\text{monoclinic}) + x_1Li^+ + x_1e^- \rightarrow Li_{x_1}MoO_2\ (\text{orthorhombic}) \quad (1)$$

https://doi.org/10.1021/acsanm.1c00218
ACS Appl. Nano Mater. 2021, 4, 4615–4622

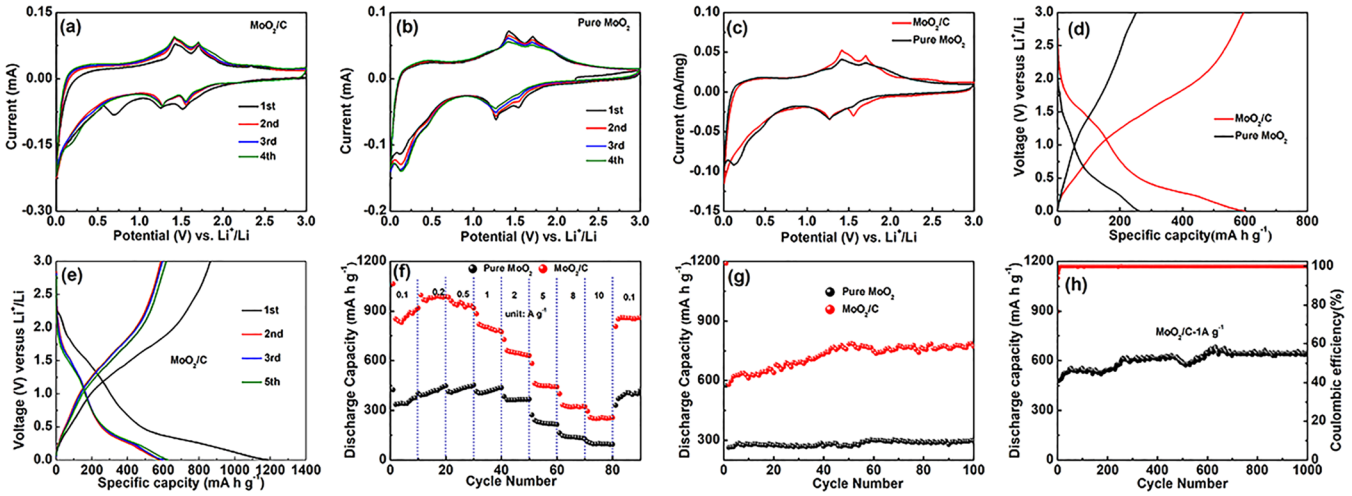

Figure 4. Electrochemical performances of the MoO_2/C composites and pure MoO_2 nanosheets as anode materials for LIBs: (a and b) CV profiles over a voltage range of 0.005−3.0 V at a scan rate of 0.1 mV s^{-1}; (c) current-normalized curves; (d) second-cycle charge/discharge profiles at 0.1 A g^{-1}; (e) charge/discharge profiles of MoO_2/C at 0.1 A g^{-1}; (f) rate performance; (g) cycling performance at 0.1 A g^{-1}; (h) cycling performance at 1 A g^{-1} of MoO_2/C composites.

$$Li_{x_1}MoO_2\ (\text{orthorhombic}) + (x_2 - x_1)Li^+ + (x_2 - x_1)e^- \rightarrow Li_{x_2}MoO_2\ (\text{monoclinic}) \quad (2)$$

$$Li_{x_2}MoO_2 + (4 - x_2)Li^+ + (4 - x_2)e^- \rightarrow Li_2O \quad (3)$$

As shown in Figure 4c, one can see that the MoO_2/C and pure MoO_2 electrodes have similar profiles; the former provided a larger integral area than the latter, which indicated that it has a higher capacity.[61] Indeed, the MoO_2/C electrode exhibits higher charge/discharge capacities than the pure MoO_2 electrode (Figure 4d), where the improved charge/discharge kinetics is most possibly due to the enhanced electrical conductivity of the composite electrode.

Figure S11 shows the first charge/discharge profiles of the MoO_2/C and pure MoO_2 electrodes at 0.1 A g^{-1}. The MoO_2/C electrode delivered a first discharge/charge capacity of 1190/863 mA h g^{-1} (CE is about 72.5%). The reversible discharge capacity of the initial cycles increased gradually for the MoO_2/C electrode, which can be attributed to the activation process of the electrodes (Figure 4e). Notably, the MoO_2/C electrode presents a remarkable rate capability, delivering the satisfactory capacities of 851, 980, 935, 809, 654, 453, 326, and 252 mA h g^{-1} at 0.1, 0.2, 0.5, 1, 2, 5, 8, and 10 A g^{-1}, respectively, compared to the pure MoO_2 electrode (Figure 4f). Furthermore, the MoO_2/C electrode delivers a better cycling stability and maintains a higher capacity of 772 mA h g^{-1} after 100 cycles at 0.1 A g^{-1} (Figure 4g). Strikingly, the long-term cycling stability tested at a high current density of 1 A g^{-1} showed a good discharge capacity of 638 mA h g^{-1} after the 1000th cycle (Figure 4h). For comparison, the pure MoO_2 electrode exhibited a markedly lower capacity of 296 mA h g^{-1} at 0.1 A g^{-1} after the 100th cycle. The cycling stability of the MoO_2/C electrode was most likely due to the abundant empty space and compliant backbone mitigating the volume change effects upon cycling, all due to the favorable porous carbon framework.

Meanwhile, the electrochemical performance of the MoS_2/C electrode was also measured. Compared with pure MoS_2 (Figure S11b), the CV curves of MoS_2/C were almost identical except in the first cycle, indicating excellent electrochemical stability (Figure S11a). The reduction peak emerging at 1.16 V corresponds to lithium intercalation between the interlayers of MoS_2 to form Li_xMoS_2 in the initial cathodic scan, and the following peak at 0.55 V represents the conversion reaction to molybdenum nanoparticles embedded in Li_2S.[35,62] During the subsequent anodic scan, two major oxidation peaks at 1.73 and 2.36 V can be observed, which are associated with the conversion of molybdenum and Li_2S to the MoS_2 phase.[35,36] After the first cycle, the CV curves exhibit good reproducibility and almost coincide, indicating high reversibility of the electrode. For the first discharge/charge curves of the MoS_2/C electrode at 1 A g^{-1}, the specific capacities were 1587/1238 mA h g^{-1}, affording a high CE of 78% (Figure S11c). The discharge/charge profiles of the second, third, and fifth cycles overlap well, indicating the high electrode reversibility. As shown in Figure S11d, the MoS_2/C electrode displays a good rate performance of 241 mA h g^{-1} at 10 A g^{-1}. The specific capacity can well recover to 913 mA h g^{-1} along with the current density after going back to 0.1 A g^{-1}. It is noted that the specific capacity of the MoS_2/C electrode exhibits good cycling stability at a high current density of 1 A g^{-1} and remains at 525 mA h g^{-1} in the 200th cycle (Figure S11e).

These results show outstanding energy storage performances of the MoO_2/C and MoS_2/C electrodes, which were even better than the leading results of MoO_2- and MoS_2-based electrodes reported in the literature (Tables S1 and S2). Moreover, the electrochemical performance of the MHCF electrode was also evaluated. Data and a detailed discussion are presented in Figure S12. Here, we only briefly draw a conclusion: the MHCF framework exhibited good rate and stable cycling performances; however, it is noteworthy that the reversible specific capacity of the MHCF electrode is drastically lower than those of the MoO_2/C and MoS_2/C electrodes, suggesting that the hierarchical interconnected conductive networks formed by the confined growth of thin MoX_2 nanosheets within the MHCFs increased the capacity performance. Meanwhile, the fact that the MoO_2/C and MoS_2/C electrodes exhibited markedly better cycling stability than the corresponding pure MX_2 suggests that the MHCF framework played a key role in mitigating the volume change

https://doi.org/10.1021/acsanm.1c00218
ACS Appl. Nano Mater. 2021, 4, 4615−4622

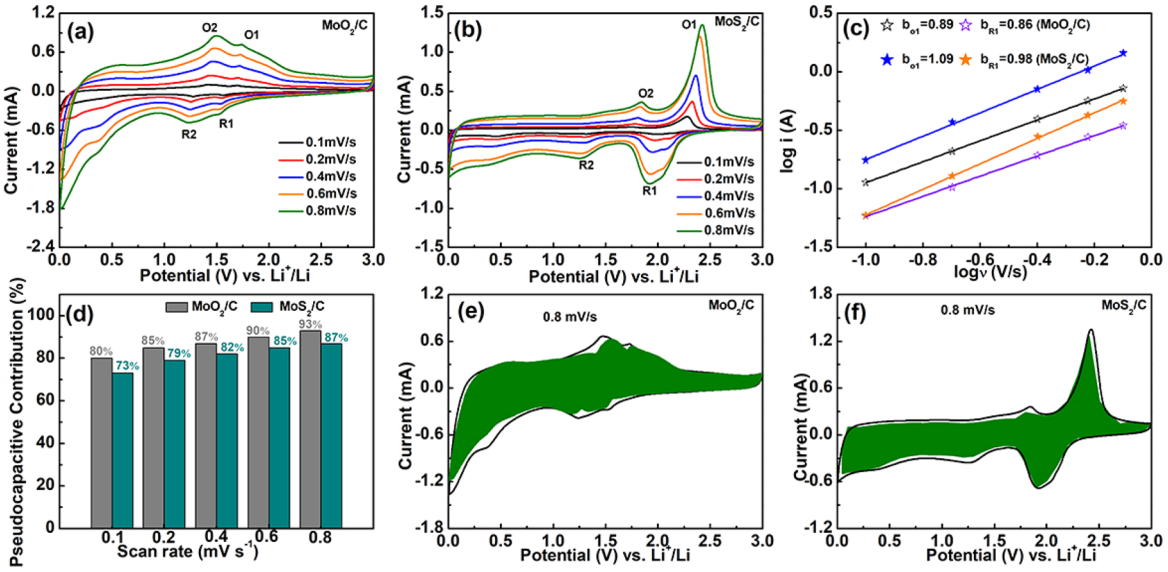

Figure 5. CV curves at different scan rates of MoO_2/C (a) and MoS_2/C (b). (c) Values of b of MoO_2/C and MoS_2/C. (d) Capacitive contribution ratio at various sweep rates of MoO_2/C and MoS_2/C. Capacitive contributions at 0.8 mV s^{-1} of MoO_2/C (e) and MoS_2/C (f).

effects upon cycling (Figures 4g and S11e). In addition, TEM examinations were adopted to investigate the structural stability of the MoX_2/C (X = O, S) electrodes. Clearly, the spherical structure was well retained, with only some small changes in the MoX_2 (X = O, S) nanosheets (Figures S13 and S14).

According to Dunn and co-workers,[63] the pseudocapacitive effect, which occurs primarily on or near the surface, promotes rapid ion diffusion of MoX_2/C electrodes with hierarchical porous structure, high specific area, and interconnected conductive networks.[64,65] Thus, we further studied the Li^+ storage kinetics by CV curves at 0.1−0.8 mV s^{-1}, so as to measure the pseudocapacitive contribution to the excellent electrochemical performance of the MoX_2/C electrodes (Figure 5a,b). The degree of capacitive effect can be qualitatively analyzed by the relationship between the scan rate (v) and peak current (i): $i = av^b$ (where a and b are both constants).[66,67] The b value ranges from 0.5 (diffusion-controlled process) to 1.0 (capacitive-controlled process), which can provide insight into the charge storage mechanism. The b value was calculated based on the slopes of the log i−log v plots (Figure 5c). The b values are all close to 1 (MoO_2/C, O1 = 0.89, R1 = 0.86; MoS_2/C, O1 = 1.09, R1 = 0.98); this phenomenon indicated that the lithium storage type was mainly from the capacitance behavior, resulting in fast reaction kinetics.

To better understand the capacitive capacity contribution to the total measured current, the total pseudocapacitive contribution can be calculated through the relationship $i = k_1v + k_2v^{1/2}$ (k_1v and $k_2v^{1/2}$ represent the capacitive and diffusion-controlled reactions at the corresponding voltage, respectively).[68,69] Visibly, Figure 5d exhibits the capacitive contributions of the MoX_2/C electrodes at 0.1−0.8 mV s^{-1}, and the capacitive contribution ratio enhances gradually from 0.1 to 0.8 mV s^{-1}. Besides, at a high scan rate of 0.8 mV s^{-1}, the capacitive contributions (green section) were calculated to be 93% (MoO_2/C, Figure 5e) and 87% (MoS_2/C, Figure 5f). The high capacitive contribution is closely related to the unique structure of MoX_2/C materials, which improves the electrochemical performance.

Taken together, the results presented above strongly confirm that the MoX_2/C composites exhibited much enhanced electrochemical performance, in comparison to pure MoX_2 and MHCFs, likely due to the following factors (Figure 6). (i)

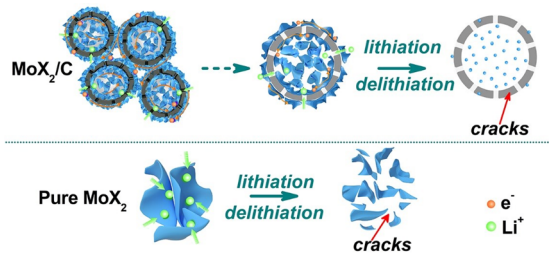

Figure 6. Schematic illustration of the transport paths of Li^+ ions and electrons and the lithiation/delithiation process in the pure MoX_2 nanosheets and MoX_2/C hierarchical composites.

The hierarchical architecture assembled from thin MoX_2 nanosheets offers short ion diffusion paths and fast Li^+ transport kinetics. (ii) The hierarchically porous carbon nanocomposites provide abundant empty space and compliant backbones to mitigate the volume change upon cycling and facilitate electrolyte ion transport and electron transfer. (iii) The interconnected conductive networks ensure the structural integrity of the nanocomposites.

CONCLUSIONS

In summary, MoX_2/C (X = O, S) hierarchical nanospheres have been successfully synthesized with a universal carbon framework template. They are composed of thin MoX_2 nanosheets encapsulated in MHCFs, with a simple hydrothermal method. Interestingly, the prepared hollow carbon framework template is universal, and it can also be used for the synthesis of $MoSe_2$/C hierarchical nanospheres. The resulting MoX_2/C hierarchical architectures can not only limit aggregation of the MoX_2 nanosheets but also alleviate volume expansion during lithium insertion/extraction. Moreover, by analysis of the reaction kinetics of MoX_2/C composites, the excellent rate capabilities and eminent cycling stability can be

https://doi.org/10.1021/acsanm.1c00218
ACS Appl. Nano Mater. 2021, 4, 4615−4622

attributed to the hierarchical porous structure and interconnected conductive networks that facilitate ion diffusion and electron transport, in comparison to pure MoX_2. Results from this study highlight the significance of the confined growth of MoX_2 nanosheets within a carbon framework in the structural engineering of molybdenum-based anode materials for LIBs.

■ ASSOCIATED CONTENT

Supporting Information

The Supporting Information is available free of charge at https://pubs.acs.org/doi/10.1021/acsanm.1c00218.

Experimental details (including the materials, synthesis of MHCFs, MoX_2/C, and pure MoX_2 materials, and characterization), SEM and TEM images, EDX elemental mappings and HRTEM images of MoS_2/C, BET results for MoX_2/C and pure MoX_2, TGA curves of the MoX_2/C composites, electrochemical performances of MoS_2/C composites, pure MoS_2 nanosheets, and MHCFs as anode materials for LIBs, and two tables showing comparisons of the electrochemical performances for lithium-ion anodes (PDF)

■ AUTHOR INFORMATION

Corresponding Authors

Ming Chen − *School of Chemistry and Chemical Engineering, Yangzhou University, Yangzhou 225002, P. R. China; Key Laboratory of Advanced Energy Materials Chemistry (Ministry of Education), College of Chemistry, Nankai University, Tianjin 300071, P. R. China;* orcid.org/0000-0002-6436-4765; Email: chenming@yzu.edu.cn

Shaowei Chen − *Department of Chemistry and Biochemistry, University of California, Santa Cruz, California 95064, United States;* orcid.org/0000-0002-3668-8551; Email: shaowei@ucsc.edu

Authors

Xiue Zhang − *School of Chemistry and Chemical Engineering, Yangzhou University, Yangzhou 225002, P. R. China; Department of Chemistry and Biochemistry, University of California, Santa Cruz, California 95064, United States*

Huajuan Ren − *School of Chemistry and Chemical Engineering, Yangzhou University, Yangzhou 225002, P. R. China*

Bin Xie − *School of Chemistry and Chemical Engineering, Yangzhou University, Yangzhou 225002, P. R. China*

Yatao Yan − *School of Chemistry and Chemical Engineering, Yangzhou University, Yangzhou 225002, P. R. China*

Guowang Diao − *School of Chemistry and Chemical Engineering, Yangzhou University, Yangzhou 225002, P. R. China;* orcid.org/0000-0001-9224-5432

Complete contact information is available at: https://pubs.acs.org/10.1021/acsanm.1c00218

Notes

The authors declare no competing financial interest.

■ ACKNOWLEDGMENTS

This work was supported by the National Natural Science Foundation of China (Grant 21773203) and the Yangzhou University International Academic Exchange Fund (Grant YZUIAEF201901003).

■ REFERENCES

(1) Cai, X.; Lai, L.; Shen, Z.; Lin, J. Graphene and graphene-based composites as Li-ion battery electrode materials and their application in full cells. *J. Mater. Chem. A* **2017**, *5* (30), 15423−15446.

(2) Song, B.; Lai, M. O.; Liu, Z.; Liu, H.; Lu, L. Graphene-based surface modification on layered Li-rich cathode for high-performance Li-ion batteries. *J. Mater. Chem. A* **2013**, *1* (34), 9954−9965.

(3) Tan, C.; Zhang, H. Two-dimensional transition metal dichalcogenide nanosheet-based composites. *Chem. Soc. Rev.* **2015**, *44* (9), 2713−2731.

(4) Wang, T.; Chen, S.; Pang, H.; Xue, H.; Yu, Y. MoS_2-based nanocomposites for electrochemical energy storage. *Adv. Sci.* **2017**, *4* (2), 1600289.

(5) Leng, K.; Chen, Z.; Zhao, X.; Tang, W.; Tian, B.; Nai, C. T.; Zhou, W.; Loh, K. P. Phase restructuring in transition metal dichalcogenides for highly stable energy storage. *ACS Nano* **2016**, *10* (10), 9208−9215.

(6) Li, H.; Shi, Y.; Chiu, M.-H.; Li, L.-J. Emerging energy applications of two-dimensional layered transition metal dichalcogenides. *Nano Energy* **2015**, *18*, 293−305.

(7) Gao, S.; Yang, L.; Shao, J.; Qu, Q.; Wu, Y.; Holze, R. Construction of hierarchical hollow MoS_2/carbon microspheres for enhanced lithium storage performance. *J. Electrochem. Soc.* **2020**, *167* (10), 100525.

(8) Zheng, M.; Tang, H.; Li, L.; Hu, Q.; Zhang, L.; Xue, H.; Pang, H. Hierarchically nanostructured transition metal oxides for lithium-ion batteries. *Adv. Sci.* **2018**, *5* (3), 1700592.

(9) Chen, L.; Jiang, H.; Jiang, H.; Zhang, H.; Guo, S.; Hu, Y.; Li, C. Mo-based ultrasmall nanoparticles on hierarchical carbon nanosheets for superior lithium ion storage and hydrogen generation catalysis. *Adv. Energy Mater.* **2017**, *7* (15), 1602782.

(10) Tang, X.; Chen, G.; Mo, Z.; Ma, D.; Wang, S.; Wen, J.; Gong, L.; Zhao, L.; Huang, J.; Huang, T.; Luo, J. Controllable two-dimensional movement and redistribution of lithium ions in metal oxides. *Nat. Commun.* **2019**, *10* (1), 2888.

(11) Zhu, S.; Chen, M.; Ren, W.; Yang, J.; Qu, S.; Li, Z.; Diao, G. Microwave assisted synthesis of α-Fe_2O_3/reduced graphene oxide as anode material for high performance lithium ion batteries. *New J. Chem.* **2015**, *39* (10), 7923−7931.

(12) Chen, M.; Shen, X.; Wu, Q.; Li, W.; Diao, G. Template-assisted synthesis of core−shell α-Fe_2O_3@TiO_2 nanorods and their photocatalytic property. *J. Mater. Sci.* **2015**, *50* (11), 4083−4094.

(13) Han, J.; Li, L.; Fang, P.; Guo, R. Ultrathin MnO_2 nanorods on conducting polymer nanofibers as a new class of hierarchical nanostructures for high-performance supercapacitors. *J. Phys. Chem. C* **2012**, *116* (30), 15900−15907.

(14) Zhang, X.; Zhou, J.; Zheng, Y.; Chen, D. $MoSe_2$−$CoSe_2$/N-doped graphene aerogel nanocomposites with high capacity and excellent stability for lithium-ion batteries. *J. Power Sources* **2019**, *439*, 227112.

(15) Kang, W.; Wang, Y.; Xu, J. Recent progress in layered metal dichalcogenide nanostructures as electrodes for high-performance sodium-ion batteries. *J. Mater. Chem. A* **2017**, *5* (17), 7667−7690.

(16) Luo, Z.; Zhou, J.; Wang, L.; Fang, G.; Pan, A.; Liang, S. Two-dimensional hybrid nanosheets of few layered $MoSe_2$ on reduced graphene oxide as anodes for long-cycle-life lithium-ion batteries. *J. Mater. Chem. A* **2016**, *4* (40), 15302−15308.

(17) Xia, Q.; Li, W.; Miao, Z.; Chou, S.; Liu, H. Phosphorus and phosphide nanomaterials for sodium-ion batteries. *Nano Res.* **2017**, *10* (12), 4055−4081.

(18) Zhu, Y.; Peng, L.; Fang, Z.; Yan, C.; Zhang, X.; Yu, G. Structural engineering of 2D nanomaterials for energy storage and catalysis. *Adv. Mater.* **2018**, *30* (15), 1706347.

(19) Tan, C.; Cao, X.; Wu, X. J.; He, Q.; Yang, J.; Zhang, X.; Chen, J.; Zhao, W.; Han, S.; Nam, G. H.; Sindoro, M.; Zhang, H. Recent advances in ultrathin two-dimensional nanomaterials. *Chem. Rev.* **2017**, *117* (9), 6225−6331.

(20) Rojaee, R.; Shahbazian-Yassar, R. Two-Dimensional Materials to Address the Lithium Battery Challenges. *ACS Nano* **2020**, *14* (3), 2628−2658.
(21) Chen, K.-S.; Balla, I.; Luu, N. S.; Hersam, M. C. Emerging Opportunities for Two-Dimensional Materials in Lithium-Ion Batteries. *ACS Energy Lett.* **2017**, *2* (9), 2026−2034.
(22) Ge, P.; Zhang, L.; Yang, Y.; Sun, W.; Hu, Y.; Ji, X. Advanced $MoSe_2$/carbon electrodes in Li/Na-ions batteries. *Adv. Mater. Interfaces* **2020**, *7* (2), 1901651.
(23) Yun, Q.; Li, L.; Hu, Z.; Lu, Q.; Chen, B.; Zhang, H. Layered transition metal dichalcogenide-based nanomaterials for electrochemical energy storage. *Adv. Mater.* **2020**, *32* (1), 1903826.
(24) Wang, D.; Liu, L.-M.; Zhao, S.-J.; Hu, Z.-Y.; Liu, H. Potential application of metal dichalcogenides double-layered heterostructures as anode materials for Li-ion batteries. *J. Phys. Chem. C* **2016**, *120* (9), 4779−4788.
(25) Roselin, L. S.; Juang, R. S.; Hsieh, C. T.; Sagadevan, S.; Umar, A.; Selvin, R.; Hegazy, H. H. Recent advances and perspectives of carbon-based nanostructures as anode materials for Li-ion batteries. *Materials* **2019**, *12* (8), 1229.
(26) Hu, X.; Zhang, W.; Liu, X.; Mei, Y.; Huang, Y. Nanostructured Mo-based electrode materials for electrochemical energy storage. *Chem. Soc. Rev.* **2015**, *44* (8), 2376−2404.
(27) Xu, L.; Hu, Y.; Zhang, H.; Jiang, H.; Li, C. Confined synthesis of FeS_2 nanoparticles encapsulated in carbon nanotube hybrids for ultrastable lithium-ion batteries. *ACS Sustainable Chem. Eng.* **2016**, *4* (8), 4251−4255.
(28) Liu, Y.; Yu, X.-Y.; Fang, Y.; Zhu, X.; Bao, J.; Zhou, X.; Lou, X. W. Confining SnS_2 ultrathin nanosheets in hollow carbon nanostructures for efficient capacitive sodium storage. *Joule* **2018**, *2* (4), 725−735.
(29) Choi, S.; Oh, M. Well-arranged and confined incorporation of PdCo nanoparticles within a hollow and porous metal-organic framework for superior catalytic activity. *Angew. Chem., Int. Ed.* **2019**, *58* (3), 866−871.
(30) Zhang, X.; Shen, C.; Wu, H.; Han, Y.; Wu, X.; Ding, W.; Ni, L.; Diao, G.; Chen, M. Filling few-layer ReS_2 in hollow mesoporous carbon spheres for boosted lithium/sodium storage properties. *Energy Storage Mater.* **2020**, *26*, 457−464.
(31) Xia, Q.; Lin, Z.; Lai, W.; Wang, Y.; Ma, C.; Yan, Z.; Gu, Q.; Wei, W.; Wang, J. Z.; Zhang, Z.; Liu, H. K.; Dou, S. X.; Chou, S. L. 2D Titania-carbon superlattices vertically encapsulated in 3D hollow carbon nanospheres embedded with 0D TiO_2 quantum dots for exceptional sodium-ion storage. *Angew. Chem., Int. Ed.* **2019**, *58* (40), 14125−14128.
(32) Zhang, X.; Zhao, R.; Wu, Q.; Li, W.; Shen, C.; Ni, L.; Yan, H.; Diao, G.; Chen, M. Petal-like MoS_2 nanosheets space-confined in hollow mesoporous carbon spheres for enhanced lithium storage performance. *ACS Nano* **2017**, *11* (8), 8429−8436.
(33) Li, X. L.; Li, T. C.; Huang, S.; Zhang, J.; Pam, M. E.; Yang, H. Y. Controllable synthesis of two-dimensional molybdenum disulfide MoS_2 for energy-storage applications. *ChemSusChem* **2020**, *13* (6), 1379−1391.
(34) Huang, H.; Cui, J.; Liu, G.; Bi, R.; Zhang, L. Carbon-coated $MoSe_2$/MXene hybrid nanosheets for superior potassium storage. *ACS Nano* **2019**, *13* (3), 3448−3456.
(35) Zhang, X.; Chen, X.; Ren, H.; Diao, G.; Chen, M.; Chen, S. Bowl-like C@MoS_2 nanocomposites as anode materials for lithium-ion batteries: enhanced stress buffering and charge/mass transfer. *ACS Sustainable Chem. Eng.* **2020**, *8* (27), 10065−10072.
(36) Wu, H.; Zhang, X.; Wu, Q.; Han, Y.; Wu, X.; Ji, P.; Zhou, M.; Diao, G.; Chen, M. Confined growth of 2D MoS_2 nanosheets in N-doped pearl necklace-like structured carbon nanofibers with boosted lithium and sodium storage performance. *Chem. Commun.* **2020**, *56* (1), 141−144.
(37) Tian, H.; Liang, J.; Liu, J. Nanoengineering carbon spheres as nanoreactors for sustainable energy applications. *Adv. Mater.* **2019**, *31* (50), 1903886.
(38) Liu, T.; Zhang, L.; Cheng, B.; Yu, J. Hollow carbon spheres and their hybrid nanomaterials in electrochemical energy storage. *Adv. Energy Mater.* **2019**, *9* (17), 1803900.
(39) Fu, A.; Wang, C.; Pei, F.; Cui, J.; Fang, X.; Zheng, N. Recent advances in hollow porous carbon materials for lithium-sulfur batteries. *Small* **2019**, *15* (10), 1804786.
(40) Chen, M.; Xu, J.-Q.; Ding, S.-N.; Shan, D.; Xue, H.-G.; Cosnier, S.; Holzinger, M. Poly(brilliant cresyl blue) electrogenerated on single-walled carbon nanotubes modified electrode and its application in mediated biosensing system. *Sens. Actuators, B* **2011**, *152* (1), 14−20.
(41) Yun, Y.; Shao, J.; Chen, Y.; Cao, Z.; Qu, Q.; Zheng, H. Nanoisland-like MoO_2 embedded in N-doped carbon via Mo−N bonds for Li-ion storage. *ACS Appl. Nano Mater.* **2019**, *2* (4), 1883−1889.
(42) Chen, Z.; Yang, T.; Shi, H.; Wang, T.; Zhang, M.; Cao, G. Single nozzle electrospinning synthesized MoO_2@C core shell nanofibers with high capacity and long-term stability for lithium-ion Storage. *Adv. Mater. Interfaces* **2017**, *4* (3), 1600816.
(43) Wang, X.; Li, H.; Li, H.; Lin, S.; Ding, W.; Zhu, X.; Sheng, Z.; Wang, H.; Zhu, X.; Sun, Y. 2D/2D 1T-MoS_2/Ti_3C_2 MXene heterostructure with excellent supercapacitor performance. *Adv. Funct. Mater.* **2020**, *30* (15), 0190302.
(44) Liu, H.; Lin, Y.; Zhang, L. Hierarchical porous MoS_2/C nanospheres self-assembled by nanosheets with high electrochemical energy storage performance. *Nanoscale Res. Lett.* **2020**, *15* (1), 199.
(45) Bai, J.; Zhao, B.; Lin, S.; Li, K.; Zhou, J.; Dai, J.; Zhu, X.; Sun, Y. Construction of hierarchical V_4C_3-MXene/MoS_2/C nanohybrids for high rate lithium-ion batteries. *Nanoscale* **2020**, *12* (2), 1144−1154.
(46) Liu, H.; Guo, H.; Liu, B.; Liang, M.; Lv, Z.; Adair, K. R.; Sun, X. Few-layer $MoSe_2$ nanosheets with expanded (002) planes confined in hollow ccarbon nanospheres for ultrahigh-performance Na-ion batteries. *Adv. Funct. Mater.* **2018**, *28* (19), 1707480.
(47) Liu, H.; Liu, B.; Guo, H.; Liang, M.; Zhang, Y.; Borjigin, T.; Yang, X.; Wang, L.; Sun, X. N-doped C-encapsulated scale-like yolk-shell frame assembled by expanded planes few-layer $MoSe_2$ for enhanced performance in sodium-ion batteries. *Nano Energy* **2018**, *51*, 639−648.
(48) Feng, Y.; Zhang, H.; Zhang, Y.; Bai, Y.; Wang, Y. Novel peapod NiO nanoparticles encapsulated in carbon fibers for high-efficiency supercapacitors and lithium-ion batteries. *J. Mater. Chem. A* **2016**, *4* (9), 3267−3277.
(49) Veerasubramani, G. K.; Park, M.-S.; Nagaraju, G.; Kim, D.-W. Unraveling the Na-ion storage performance of a vertically aligned interlayer-expanded two-dimensional MoS_2@C@MoS_2 heterostructure. *J. Mater. Chem. A* **2019**, *7* (42), 24557−24568.
(50) Zhou, L.; Wu, H. B.; Wang, Z.; Lou, X. W. Interconnected MoO_2 nanocrystals with carbon nanocoating as high-capacity anode materials for lithium-ion batteries. *ACS Appl. Mater. Interfaces* **2011**, *3* (12), 4853−7.
(51) Liu, C.; Luo, S.; Huang, H.; Zhai, Y.; Wang, Z. Direct growth of MoO_2/reduced graphene oxide hollow sphere composites as advanced anode materials for potassium-ion batteries. *ChemSusChem* **2019**, *12* (4), 873−880.
(52) Bhaskar, A.; Deepa, M.; Narasinga Rao, T. MoO_2/multiwalled carbon nanotubes (MWCNT) hybrid for use as a Li-ion battery anode. *ACS Appl. Mater. Interfaces* **2013**, *5* (7), 2555−66.
(53) Hou, M.; Qiu, Y.; Yan, G.; Wang, J.; Zhan, D.; Liu, X.; Gao, J.; Lai, L. Aging mechanism of MoS_2 nanosheets confined in N-doped mesoporous carbon spheres for sodium-ion batteries. *Nano Energy* **2019**, *62*, 299−309.
(54) Yang, L. C.; Gao, Q. S.; Tang, Y.; Wu, Y. P.; Holze, R. MoO_2 synthesized by reduction of MoO3 with ethanol vapor as an anode material with good rate capability for the lithium ion battery. *J. Power Sources* **2008**, *179* (1), 357−360.
(55) Liu, J.; Tang, S.; Lu, Y.; Cai, G.; Liang, S.; Wang, W.; Chen, X. Synthesis of Mo_2N nanolayer coated MoO_2 hollow nanostructures as high-performance anode materials for lithium-ion batteries. *Energy Environ. Sci.* **2013**, *6* (9), 2691.

https://doi.org/10.1021/acsanm.1c00218
ACS Appl. Nano Mater. 2021, 4, 4615−4622

(56) Zhao, C.; Yu, C.; Zhang, M.; Huang, H.; Li, S.; Han, X.; Liu, Z.; Yang, J.; Xiao, W.; Liang, J.; Sun, X.; Qiu, J. Ultrafine MoO_2-carbon microstructures enable ultralong-life power-type sodium ion storage by enhanced pseudocapacitance. *Adv. Energy Mater.* **2017**, *7* (15), 1602880.
(57) Palanisamy, K.; Kim, Y.; Kim, H.; Kim, J. M.; Yoon, W.-S. Self-assembled porous MoO_2/graphene microspheres towards high performance anodes for lithium ion batteries. *J. Power Sources* **2015**, *275*, 351−361.
(58) Yang, L.; Liu, L.; Zhu, Y.; Wang, X.; Wu, Y. Preparation of carbon coated MoO_2 nanobelts and their high performance as anode materials for lithium ion batteries. *J. Mater. Chem.* **2012**, *22* (26), 13148.
(59) Yang, L. C.; Sun, W.; Zhong, Z. W.; Liu, J. W.; Gao, Q. S.; Hu, R. Z.; Zhu, M. Hierarchical MoO_2/N-doped carbon heteronanowires with high rate and improved long-term performance for lithium-ion batteries. *J. Power Sources* **2016**, *306*, 78−84.
(60) Tang, Q.; Shan, Z.; Wang, L.; Qin, X. MoO_2−graphene nanocomposite as anode material for lithium-ion batteries. *Electrochim. Acta* **2012**, *79*, 148−153.
(61) Fei, R.; Wang, H.; Wang, Q.; Qiu, R.; Tang, S.; Wang, R.; He, B.; Gong, Y.; Fan, H. J. In situ hard-template synthesis of hollow bowl-like carbon: A potential versatile platform for sodium and zinc ion capacitors. *Adv. Energy Mater.* **2020**, *10* (47), 2002741.
(62) Hu, S.; Chen, W.; Zhou, J.; Yin, F.; Uchaker, E.; Zhang, Q.; Cao, G. Preparation of carbon coated MoS_2 flower-like nanostructure with self-assembled nanosheets as high-performance lithium-ion battery anodes. *J. Mater. Chem. A* **2014**, *2* (21), 7862.
(63) Wang, J.; Polleux, J.; Lim, J.; Dunn, B. Pseudocapacitive contributions to electrochemical energy storage in TiO_2 nanoparticles. *J. Phys. Chem. C* **2007**, *111* (40), 14925−14931.
(64) Augustyn, V.; Come, J.; Lowe, M. A.; Kim, J. W.; Taberna, P. L.; Tolbert, S. H.; Abruna, H. D.; Simon, P.; Dunn, B. High-rate electrochemical energy storage through Li^+ intercalation pseudocapacitance. *Nat. Mater.* **2013**, *12* (6), 518−522.
(65) Sun, B.; Lou, S.; Qian, Z.; Zuo, P.; Du, C.; Ma, Y.; Huo, H.; Xie, J.; Wang, J.; Yin, G. Pseudocapacitive Li^+ storage boosts ultrahigh rate performance of structure-tailored $CoFe_2O_4$@Fe_2O_3 hollow spheres triggered by engineered surface and near-surface reactions. *Nano Energy* **2019**, *66*, 104179.
(66) Zhang, S.; Wang, G.; Zhang, Z.; Wang, B.; Bai, J.; Wang, H. 3D graphene networks encapsulated with ultrathin SnS nanosheets@ hollow mesoporous carbon spheres nanocomposite with pseudocapacitance-enhanced lithium and sodium storage kinetics. *Small* **2019**, *15* (14), 1900565.
(67) Shen, Q.; Jiang, P.; He, H.; Chen, C.; Liu, Y.; Zhang, M. Encapsulation of $MoSe_2$ in carbon fibers as anodes for potassium ion batteries and nonaqueous battery-supercapacitor hybrid devices. *Nanoscale* **2019**, *11* (28), 13511−13520.
(68) Brezesinski, T.; Wang, J.; Tolbert, S. H.; Dunn, B. Ordered mesoporous α-MoO_3 with iso-oriented nanocrystalline walls for thin-film pseudocapacitors. *Nat. Mater.* **2010**, *9* (2), 146−51.
(69) Cook, J. B.; Kim, H.-S.; Yan, Y.; Ko, J. S.; Robbennolt, S.; Dunn, B.; Tolbert, S. H. Mesoporous MoS_2 as a transition metal dichalcogenide exhibiting pseudocapacitive Li and Na-ion charge storage. *Adv. Energy Mater.* **2016**, *6* (9), 1501937.

https://doi.org/10.1021/acsanm.1c00218
ACS Appl. Nano Mater. 2021, 4, 4615−4622